Fabrication and Hall Measurements of Hydrogen-Terminated Diamond 2DHG Devices

SNF Community Service Project Final Report
Ricardo Peterson (rp3@stanford.edu)
Mentor: Xiaoqing Xu (steelxu@stanford.edu)

I. Introduction & Motivation

As a semiconductor material, diamond has exceptional figures of merit due to its wide band gap, high breakdown voltage, high thermal conductivity, and high carrier mobility [1]. The combination of wide band gap and high electron and hole mobilities is rare among semiconductor materials, which makes diamond an attractive candidate for high power electronics. However, doping of diamond has been a challenge, owing to its large activation energies for dopants (0.37 eV for p-type) [2], where one in 10^4 boron dopants is activated at room temperature. For this reason, hydrogen-terminated diamond (H:Diamond) has been studied as an alternative conduction mechanism. It has been demonstrated that when H:Diamond is exposed to air, atmospheric molecules adsorb onto the surface and induce a two-dimensional hole gas (2DHG), achieving a hole density of 10^{12} – 10^{13} cm^{-2} and a hole mobility of 50 – 150 cm^2 / (V·s) [3, 4]. An electrochemical surface transfer doping model is most commonly invoked to explain this surface conduction mechanism [5]. In this model, electron transfer occurs from the top of the surface diamond's valence band to lower accessible energy states in the atmospheric adsorbates. This causes an alignment of the Fermi energy, which is near or below the top of valence band at the H:Diamond surface. Thus, a hole gas is induced, and a compensating sheet of negative charge is formed in the first mono-layer of the air-adsorbates [6, 7].

At temperatures exceeding ~60 C, however, the air-adsorbates begin to thermally desorb from the diamond surface, thus causing the 2DHG to collapse [4, 8]. This is unfortunate since the value of diamond-based electronics stems from its potential to operate robustly at high temperatures. For this reason, surface passivation of H:Diamond has been explored as a solution. It was found by Kawarada et al. that Al_2O_3 passivation stabilizes the hole conduction above 400 C [9]. Since then, other dielectric layers such as HfO_2 have been used to passivate the H:Diamond surface [10]. Moreover, transition-metal oxides (TMOs) with high work functions such as WO_3, V_2O_5, and MoO_3 have been shown to act as efficient electron acceptors [4, 11], thus inducing much higher 2DHG densities.

In this project, we use the Stanford Nanofabrication Facility to fabricate and test H:Diamond devices. We discuss the largest challenges faced during this fabrication process, and the solutions devised to overcome them. Both Hall-effect devices and field-effect transistors are fabricated and tested using the LakeShore 8404 Hall System and a standard probe station. All three measurement heads were used on the LakeShore: the Room Temperature (RT), Closed-Cycle Refrigerator (CCR), and Oven. To become familiar with the Hall system, preliminary measurements were made using pre-fabricated GaN-based devices. This project resulted in the development of a fabrication process for diamond-based devices, which, to the authors' knowledge, has not been done at SNF. Moreover, statement of procedures were put together for the operation of the LakeShore system, which is one of SNF's newest tools, offering users the ability to characterize the conduction properties of their materials at a wide range of temperatures.

II. Objectives

The objective of this project was three-fold. The first was to develop a fabrication process of H:Diamond based devices using SNF's facilities. The second was to operate the Lakeshore Hall System and analyze the results. The third was to document the fabrication process (i.e., a run-sheet), and the operation of the Hall system (i.e., a statement of procedure, or SOP).

This project was performed in two fabrication phases. In each phase, devices were fabricated on multiple substrates of 3 x 3 mm single-crystal diamond. Analyses in the form of standard inspections and characterizations were done to evaluate the quality of the process.

III. Fabrication Process

In this section we detail the fabrication process, which was developed over five iterations of diamond substrates. Each posed unique challenges, and solutions were implemented accordingly. The details of this process is explained below.

A. Hydrogenation process

At present moment, the hydrogenation treatment is the only fabrication step that is outside of the capabilities of SNF. In order to fabricate devices on diamond, the surface must be treated with a hydrogen plasma, which will create the hydrogen-termination and induce a *p*-type conductive surface. The substrates were CVD-grown, 250 μm-thick, 3x3 mm single-crystal (001) diamond, obtained from Element Six Ltd. The diamond surfaces were treated at the University of California at Davis using a microwave CVD reactor. The hydrogen plasma power and pressure were 1.35 kW and 30 torr, respectively. This treatment lasted for 30 min with a surface temperature measured at 910 C.

B. Final fabrication process

The fabrication process is explained below and is followed by a schematic. A detailed run sheet is available in Appendix A.

(i) Hydrogen-terminate the diamond surface under a high-power plasma in a microwave CVD-chamber for 30 min.
(ii) Ti/Pt/Au (5/20/20 nm) bond pads were patterned and deposited via e-beam evaporation, followed by the standard lift-off technique. To ensure good adhesion and ease of wirebonding, the patterned bond pad regions were oxygen-terminated in a 100 W O-plasma for 90 seconds prior to the metal evaporation.
(iii) Au ohmic contacts (80 nm) were deposited using the same procedure as the prior step with the exception of the O-plasma. The Au overlaid the bondpads while making contact with the H-terminated surface.
(iv) Isolation regions were patterned and exposed to 100 W O-plasma for 90 seconds. This step defined the active regions and electrically isolated the devices.
(v) The surface was passivated with 25 nm of Al2O3 via atomic layer deposition at 250 C. The oxide interface provides acceptor states for the 2DHG formation, and also stabilizes the 2DHG over time and over a wide range of temperatures [4, 16].

(vi) The oxide was etched at the bond pad regions by submerging the patterned sample in a 20:1 BOE solution for 60 seconds.

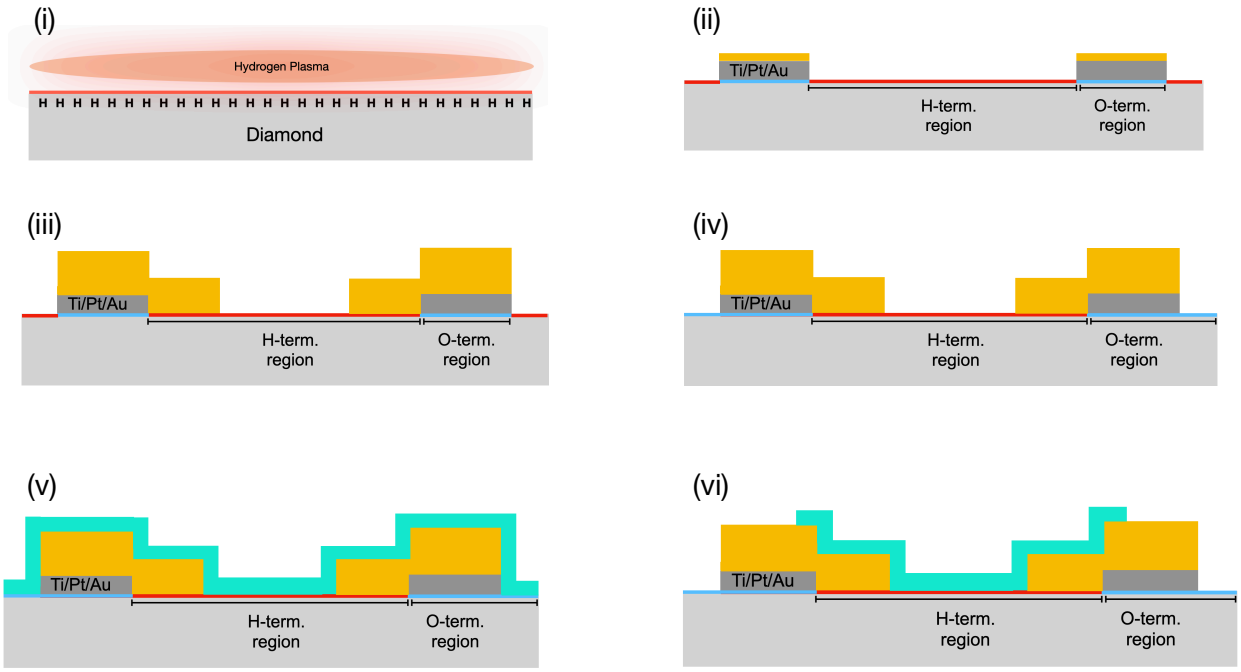

Fig. 1. Final fabrication process, summarized in six steps. A detailed run sheet is available in Appendix A.

C. Challenges and solutions

1. Poor adhesion

In a pristine surface of (100) diamond, the carbon atoms are reconstructed such that the four outermost valence orbitals are bonded, thus forming C-C dimers. The effect of the hydrogen termination process is to break these dimers and form a dipole with each surface carbon atom. To achieve a uniform interface of C-H dipoles, exposure to elemental hydrogen is performed under highly energetic conditions (i.e., a high temperature and plasma power). Since the superficial carbon atoms posses only one dangling bond, the reaction with hydrogen and its single 1s orbital effectively leaves the entire surface passivated. Moreover, given the small size of the hydrogen atom, the C-H bond length is very small (~1 Å), which results in a great force of attraction between the nuclei and forms a highly stable bond. This is an unfortunate reality in the context of metal electrodes, whether they be Schottky or ohmic. When evaporated, an interfacial metal is rather inert to the C-H surface, regardless of the delta in electronegativity. This results in a relatively large distance between the metal atoms and the C-H surface, where even mild external forces can be sufficient to physically lift the metal layer. Figure 2 (left) shows this phenomenon. After spraying the surface with solvents, the Ti/Pt/Au layer was lifted.

Strong adhesion is paramount for the structural integrity of the device. Moreover, probing and wirebonding is either very difficult or practically impossible with poor adhesion. The solution to this is to treat the surface with a 100 W oxygen plasma for 60 seconds prior to Ti/Pt/Au evaporation. This renders the surface oxygen-terminated, which reacts strongly with the interfacing Ti. As shown in Figure 2 (right), the outer perimeter

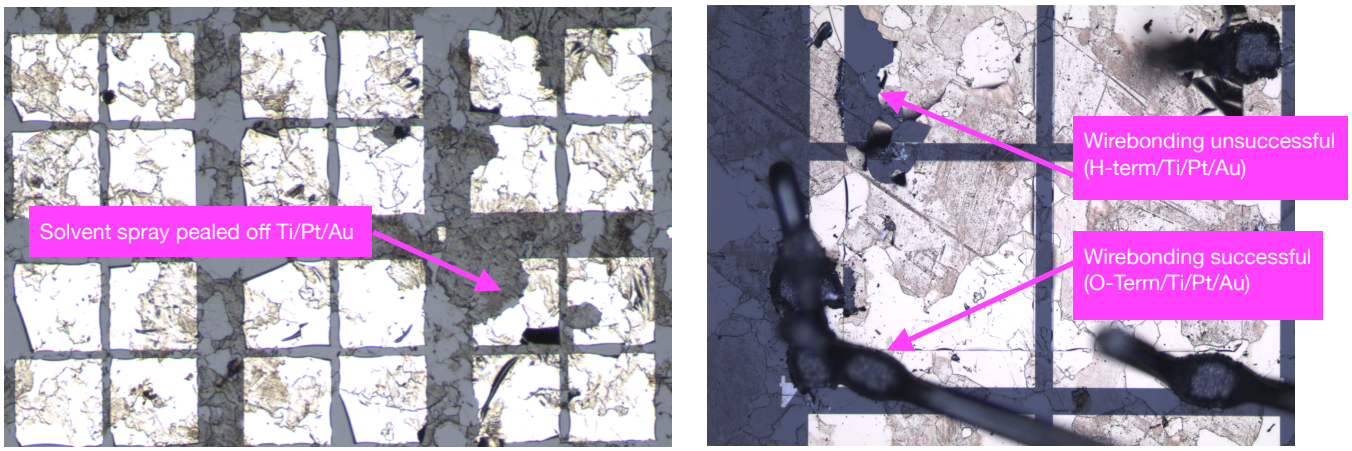

Fig. 2. (left) Ti/Pt/Au layer on hydrogen-terminated diamond (polycrystalline in this case, which explains the apparent grain boundaries). The result of spraying with solvents was sufficient to peal off the metal layers. (right) Another Ti/Pt/Au layer was deposited, this time with oxygen-plasma exposure prior to evaporation+lift-off. The result was strong adhesion, thus allowing for wirebonding.

was treated with oxygen-plasma prior to metal deposition. The resulting adhesion was strong enough for wirebonding.

2. Photoresist residue

During the experimental phases of the fabrication process, it was discovered that a thin film of resist residue remained after stripping the photoresist (SPR 3612), as shown in Figure 3. This resist remained even after submersion in more aggressive strippers such as Microposit remover 1165 or SRS 100 at elevated temperatures. The boundary between the H-terminated and O-terminated surface appears to strongly adhere to the resist, which is likely aided by the highly polar hydroxyl groups along the boundary. It is worthwhile noting that the residue shown in Figure 3 is not apparent under an optical microscope, and was only obvious under the elemental contrasting intrinsic to SEM images. The solution to this was to ultimately refrain from exposing the surface to SPR 3612, and to strictly use LOL2000/SPR 3612 double layers, even for lithography steps that do not involve a metal lift-off. The stripping process for this double layer (submersion in remover 1165 for 1 hour) resulted in negligible residue.

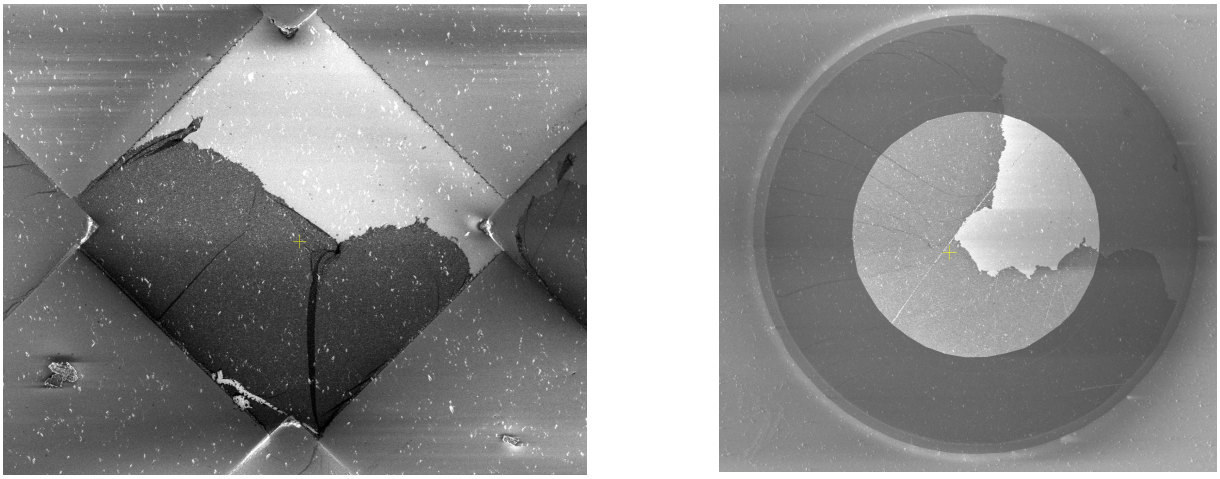

Fig. 3. SEM image of a Hall-effect device (left) and MOSCAP (right). Dark residue is apparent, which is believed to be remnants of SPR 3612 that failed to dissolve during resist stripping.

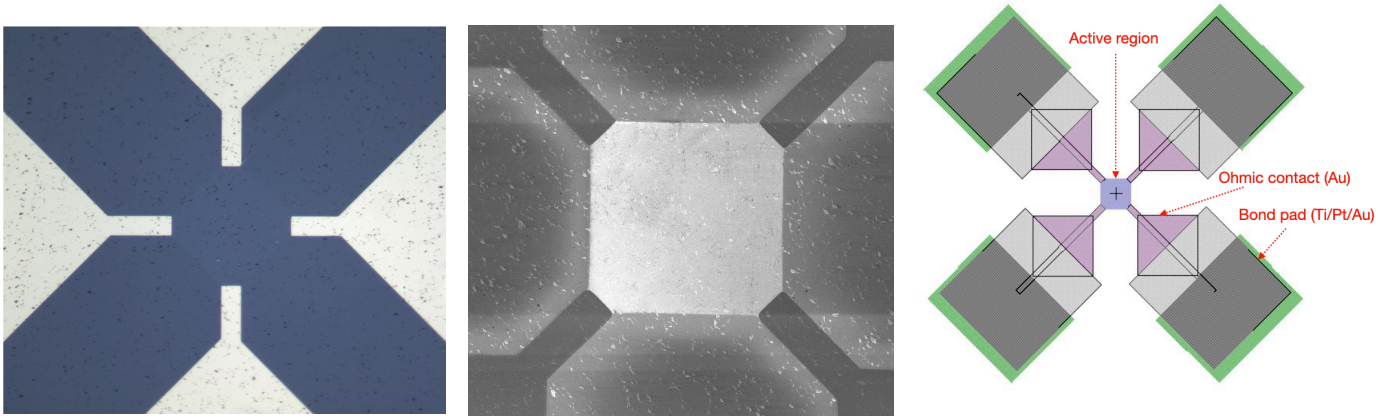

Fig. 4. (left) Optical microscope and (center) SEM image of Hall-effect device. The bright square at the center of the SEM image is the active (conductive) region of the device. (right) Layout of the Hall-effect device with labeled regions.

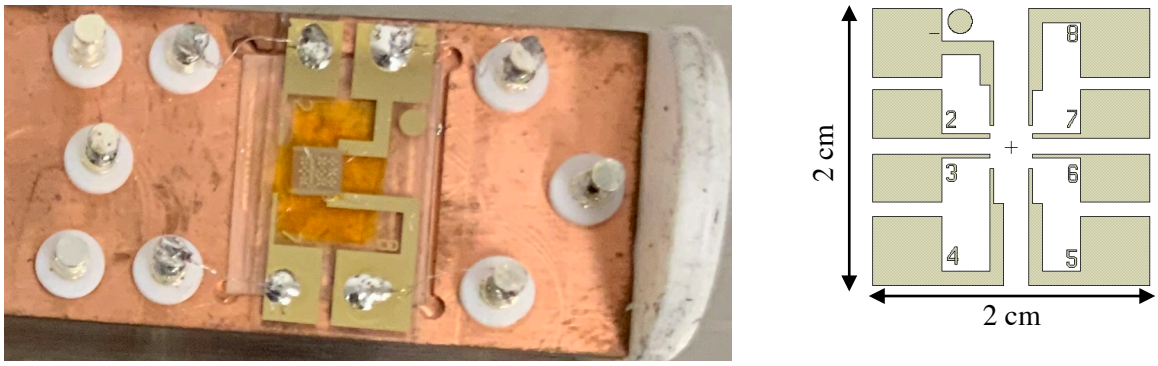

Fig. 5. (left) Diamond substrate mounted on the insert to the Lakeshore's CCR. The diamond is first wire bonded onto enlarged Ti/Pt/Au leads fabricated on a quartz wafer, the layout of which is shown (right). With the use of a wirebonder, this allows substrates of all sizes to be measured on the Lakeshore system.

IV. Results

Here we summarize the result of this work. The final device architecture and electrical characteristics are presented. We finalize this report with a short overview of characterized GaN HEMT, which are standard devices used for Hall-effect measurements.

A. Device Architecture

Images of the devices from a scanning electron microscope (SEM) and optical microscope (OM) is presented in Figure 4. The bright square at the center of the SEM image is the H-terminated active region. Note the bright and dark spots (shown in the SEM and OM image, respectively), these are etched pits caused by the H-plasma exposure. Also note that no residue is observed as in Fig. 3, which is owed to using a LOL2000 / SPR 3612 bilayer for all lithography steps, as opposed to exposing the surface to 3612 directly.

For the Hall-effect device, the bond pad region is a Ti/Pt/Au trilayer with 5/20/100 nm thicknesses, the ohmic region is an 80 nm thick layer of Au, and the active region is 50 x 50 um.

For the FET device, the width and length of the channel (show in Fig. 7) is 100 and 30 um, respectively. The gate electrode is a Ti/Pt bilayer with 20 / 20 nm thicknesses and the gate length is 5 um.

B. Hall-effect characterization

As shown in Fig. 4, the diamond substrate was adhered onto a quartz mount with enlarged metal pads, as shown in Figure 5. The enlarged pads were patterned and evaporated onto a 4-inch quartz wafer. The die were later diced in half to fit the mounting setup of the Hall system, and resulted in about 26 individual quartz die. The Hall-effect device was then wire bonded onto the larger pads, which made the soldering process possible. Since the bond pads on the diamond substrate are on the order of 100 um, enlarging the pads was necessary for mounting the device onto the Hall system. The availability of these mounts makes the Lakeshore system far more versatile as it allows for the characterization of small geometries.

Figure 6(left) shows the experimental hole mobility extracted by Hall-effect measurements of two devices on separate diamond substrates. The measurements were swept from low to high temperatures, thus yielding a $\mu(T)$ function. The largest quantitative difference between the two devices is their sheet carrier concentrations, which were measured to be 5.5e12 and 2.4e12 cm^{-2}. As shown in the figure, the concentration difference has a pronounced effect on the mobility, especially at lower temperatures. The reasoning for this is explained in great detail in the manuscript that was submitted as a result of this work [12]. In brief, conductive holes in the 2D channel are perturbed by fields induced by ionized impurities and surface disorder related to the C-H dipoles. The rate of this scattering is much higher near the top of the valence band. Thus, as the Fermi level decreases with respect to the valence band maximum, the overall scattering rate is enhanced. This explains why the mobility for the lower carrier concentration is lower. This is particularly true at low temperatures, where a higher proportion of holes occupy states nearer to the valence band maximum (due to the narrowing of the Fermi function). Figure 6(right) is a plot from the submitted manuscript, which shows the developed scattering model fitted to the experimental data of this work and other references. It is clear that the experimental data from this work is in the anticipated range of mobility values.

A detailed statement of procedures for the operation of the LakeShore system is available in Appendix A.

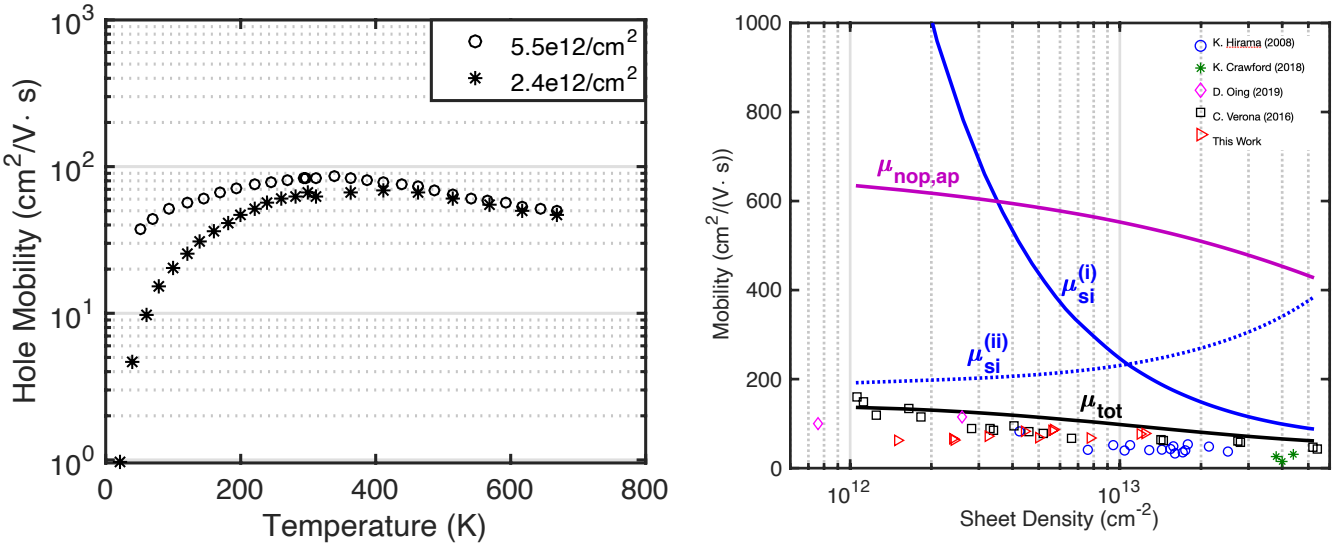

Fig. 6. (left) Hall mobility measurements at a wide range of temperatures. This was done for two substrates with distinct sheet carrier densities. (right) Plot from a recently submitted manuscript, where a scattering model was developed and fitted to the experiment data of this work, and that of other authors. It is clear that the experimental data from this work is in the anticipated range.

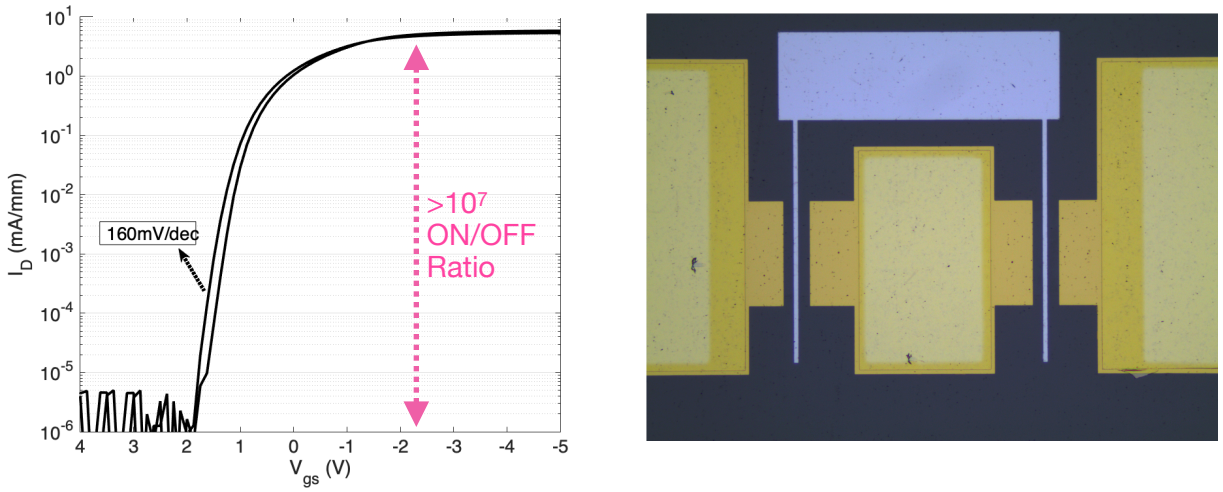

Fig. 7. (left) ID / VG curves for two diamond FETs. The ON/OFF ratio exceeds 10^7, and the subthreshold swing is 160 mV/decade. This is promising behavior for diamond-based transistors. (right) An OM image of the two FETs.

C. FET characterization

The operational stability of diamond at high temperatures and high power makes robust diamond-based FETs a desirable feat. Thus, diamond FETs were fabricated alongside the Hall-effect devices. Only one extra lithography step was required to realize the FETs, which was the gate metal deposition. The width and length of the FET channel is 100 um and 30 um, respectively. The gate electrode is a Ti/Pt bilayer with 20 / 20 nm thicknesses and a gate length of 5 um.

Since the saturation current values are dictated by the electrical properties such as mobility and sheet carrier concentration, this analysis is ignored here since such properties were already extracted via Hall-effect measurements. Other characteristics, such as the ON/OFF ratio and subthreshold swing, are shown in Figure 7 for two FETs. The ON/OFF ratios are measured to exceed 10^7 and the sub threshold swings are around 160 mV/decade. These values demonstrated promising FET behavior, and is worthwhile investigating for high temperature and high power applications. One suggestion is to utilize different passivation layers such as WO3 and MoO3. These oxides have shown to reduce the sheet resistance due to a much higher carrier density. Thus, there are opportunities to design a much more robust diamond-based FET using facilities at SNF.

D. Measurement of GaN-based HEMTs

Although the center of this project was diamond-based devices, GaN-based devices were characterized as they were readily available at the time the LakeShore system was ready to operate. Moreover, GaN devices are much more mature. The first GaN device was fabricated at SNF on AlGaN/GaN substrates grown in the aix-ccs MOCVD in the SNF MOCVD lab by Xiaoqing Xu, Minmin Hou, and Hongyun So. The second GaN device was also fabricated at SNF on InAlN/GaN substrates purchased from NTT Advanced Technology Corporation. Preliminary InAlN/GaN recipes also exist in the SNF MOCVD lab, developed by Xiaoqing Xu, Ricardo Peterson, and Thomas Heuser, although further work must be done to achieve state-of-the-art performance.

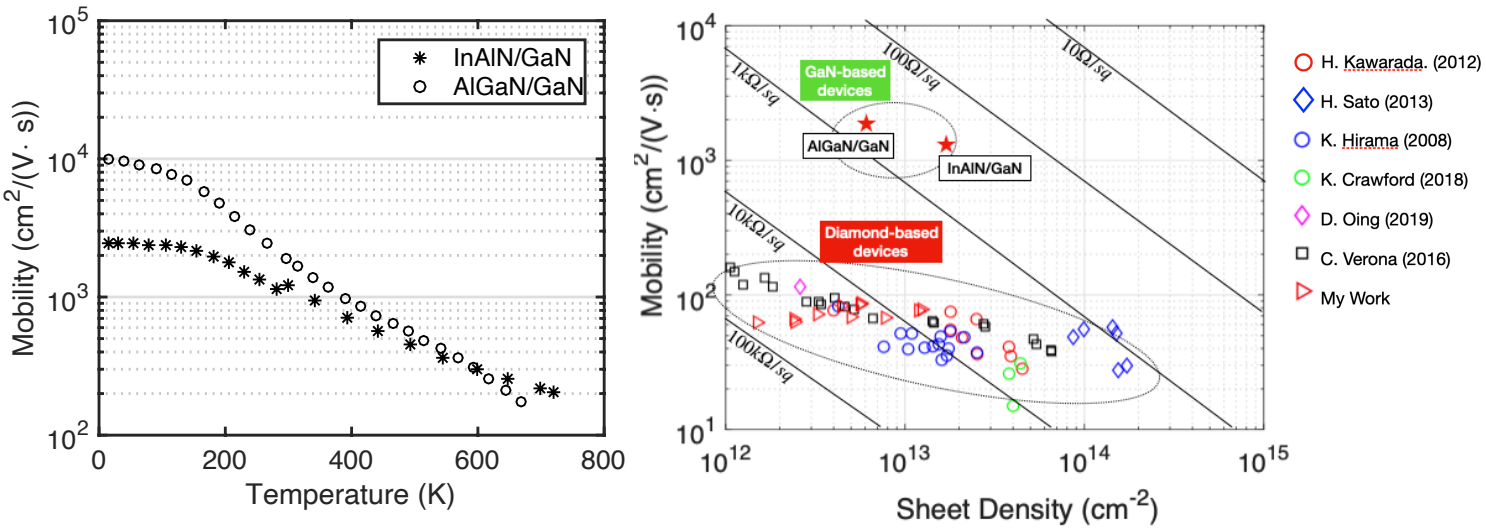

Fig. 8. (left) Mobility v.s. temperature for AlGaN/GaN and InAlN/GaN Hall-effect devices. It is shown that the mobility for AlGaN/GaN [14] is considerably higher, especially at low temperatures. InAlN/GaN [13], on the other hand, exhibits a much larger sheet carrier concentration (right).

As shown in Figure 8(left), Hall mobility measurements of the AlGaN/GaN and InAlN/GaN devices were swept from 15 K to ~650 K [13, 14]. A standard $\mu(T)$ function was measured, where the mobility decreases at high temperatures (due to optical phonon scattering), and increases at lower temperatures (due to the suppression of acoustic phonon scattering). The flattening of the mobility curve at low temperatures is attributed to scattering induced by impurities, alloys, or spatial roughness along the 2D channel. This $\mu(T)$ can be assorted into separate temperature regimes and studied carefully, which allows us to make inferences about the quality of the material and the device architecture. Shown in Figure 8(right) are data points of the mobility with respect to sheet carrier concentration for diamond and the GaN-based devices. From this analysis, it is clear that GaN-based devices have superior performance, owing to the lower sheet resistance. It is for this reason that further work is needed to boost the conduction of H:Diamond devices, which is largely what motivated the theme of this project and the submitted manuscript [12].

V. Conclusion and Future Work

In conclusion we have used the SNF facilities to fabricate and test H:Diamond devices, both Hall-effect and FETs. We discussed challenges and solutions faced during the fabrication process. The LakeShore Hall System was operated extensively during this project, and detailed statement of procedures have been developed for the rest of the SNF community who is interested in Hall-effect measurements. The results of the Hall-effect measurements were presented both for H:Diamond and GaN-based devices. The results for H:Diamond FETs were also reported and showed promising device behavior. The fabrication run-sheet for the H:Diamond devices, as well as the LakeShore statement of procedures, are all listed in Appendix A.

Although this work has been thorough in fabricating H:Diamond devices and understanding the operation of the LakeShore system, there is still much work to be done. From the fabrication standpoint, passivation of transition metal oxides would induce a much higher sheet carrier concentrations. The Fiji ALD tools, for instance, have been used to deposit MoO3 and WO3. In general, any deposition capabilities of oxides with very high work functions should increase the hole carrier concentration. Moreover, a detailed analysis of these oxides and their quality for robust FET operation must also be done. From the standpoint of the LakeShore, operation in a gate-bias configuration can be highly advantageous for many users. In this project, the LakeShore was solely operating in current bias mode

with a voltage read-out, as this is all that is required for Hall-effect measurements. However, for FET transfer characteristics, gate bias is needed. The simplest solution is to purchase the "Gate Bias" mode by LakeShore, which comes with a sensitive voltage supply and license to operate it using the LakeShore software. Another crude work-around (though not recommended) is to use an external voltage supply and manually connect it to the coaxial inputs of the LakeShore heads.

VI. Acknowledgements

This project would not have been possible without the mentorship of Dr. Xiaoqing Xu and the technical expertise of Graham Ewing. Connor McClellan's involvement has also been essential in the operation of the LakeShore system. Special thanks is also given to Mohamadali Malakoutian from Prof. Srabanti Chowdhury's group, for hydrogen-terminating the diamond substrates at UC Davis. The rest of the SNF staff involved in ramping up the LakeShore system and maintaining the SNF equipment was also essential for the work reported here.

References

[1] M. W. Geis, T. C. Wade, C. H. Wuorio, T. H. Fedynyshyn, B. Duncan, M. E. Plaut, J. O. Varghese, S. M. Warnock, S. A. Vitale, and M. A. Hollis, physica status solidi (a) **215**, 1800681 (2018).

[2] A. T. Collinsand A. W. S. Williams, Journal of Physics C: Solid State Physics **4**, 1789 (1971).

[3] K. Hirama, K. Tsuge, S. Sato, T. Tsuno, Y. Jingu, S. Yamauchi, and H. Kawarada, Applied Physics Express **3**, 044001 (2010).

[4] C. Verona, W. Ciccognani, S. Colangeli, E. Limiti, M. Marinelli, and G. Verona-Rinati, Journal of Applied, Physics **120**, 025104 (2016).

[5] F. Maier, M. Riedel, B. Mantel, J. Ristein, and L. Ley, Phys. Rev. Lett. **85**, 3472 (2000).

[6] H. Kawarada, Surface Science Reports **26**, 205 (1996).

[7] K. Tsugawa, H. Umezawa, and H. Kawarada, Japanese Journal of Applied Physics **40**, 3101 (2001).

[8] M. Riedel, J. Ristein, and L. Ley, Phys. Rev. B **69**, 125338 (2004).

[9] H. Kawarada, H. Tsuboi, T. Naruo, T. Yamada, D. Xu, A. Daicho, T. Saito, and A. Hiraiwa, Applied Physics Letters **105**, 013510 (2014).

[10] J. W. Liu, M. Y. Liao, M. Imura, H. Oosato, E. Watanabe, and Y. Koide, Applied Physics Letters **102**, 112910 (2013).

[11] S. A. O. Russell, L. Cao, D. Qi, A. Tallaire, K. G. Craw-ford, A. T. S. Wee, and D. A. J. Moran, Applied Physics Letters **103**, 202112 (2013).

[12] R. Peterson, M. Malakoutian, X. Xu, C. Chapin, S. Chowdhury, D. G. Senesky, "Analysis of the Mobility-Limiting Mechanisms of the Two-Dimensional Hole Gas on Hydrogen-Terminated Diamond," https://arxiv.org/abs/2003.08007, 2020.

[13] H. S. Alpert, K. M. Dowling, C. A. Chapin, A. S. Yalamarthy, S. R. Benbrook, H. Köck, U. Ausserlechner, and D. G. Senesky, IEEE Sensors, **19,** 3640, (2019).

[14] M. Hou, S. Jain, H. So, T. Heuser, X. Xu, and D. G. Senesky, Journal of Applied Physics, **122**, 19, 195102, (2017).

Appendix A

Fabrication run-sheet for the H:Diamond devices:
https://drive.google.com/file/d/1hC2JigOubLgCAGcsHyp-fSmymgk-yp1-/view?usp=sharing

Statement of Procedure for RT operation:
https://drive.google.com/file/d/19LQe9vZPQNEJMzsU8f14C3ITRLcGjYc0/view?usp=sharing

Statement of Procedure for CCR operation:
https://drive.google.com/file/d/1f0WEtzQtoAqQ7Ua2Pgfu4fANTfC5wAaC/view?usp=sharing

Statement of Procedure for Oven operation:
https://drive.google.com/file/d/1SY3g5gVECH_SPPFKPGJi7ILNVktJ8mR6/view?usp=sharing